Role of Passive Microwave Remote Sensing in Improving Flood Forecasts

Rajat Bindlish, *Senior Member, IEEE*, Wade T. Crow, and Thomas J. Jackson, *Fellow, IEEE*

***Abstract*—Accurate information concerning antecedent soil moisture conditions is a key source of hydrologic forecasting skill for regional-scale flooding events occurring over time scales of days to weeks. Remotely sensed surface soil moisture observations are a viable source of such information and can potentially improve flood peak timing and magnitude forecasting in such events. C- and X-band brightness temperature data from the Advanced Microwave Scanning Radiometer (AMSR-E) aboard NASA's Aqua satellite are used here to demonstrate the potential for improving streamflow forecasts by using remotely sensed surface soil moisture during a flooding event in northeastern Australia (Queensland) during January–February 2004. An analysis of AMSR-E brightness temperature imagery reveals a clear anomaly of low AMSR-E brightness temperatures (i.e., high soil moisture conditions) over the affected areas in the four- to five-day period preceding peak streamflow conditions. Land surface conditions are a remotely detectable precursor to subsequent downstream flooding. Use of a simple adaptive model demonstrates that AMSR-E passive microwave observations can add skill to streamflow forecasts during the event.**

***Index Terms*—Floods, hydrology, microwave remote sensing, rainfall–runoff modeling, soil moisture.**

I. Introduction

FLOODS are, by a large margin, the most costly of natural hazards in terms of both human lives and property damage [1], and an increased frequency and severity of floods is commonly cited as one of the potential risks of climate and land-use change [2]. Soil moisture is the key state variable for land surface hydrology; it controls the proportion of rainfall that infiltrates, runs off, or evaporates from the land surface. Soil moisture also integrates precipitation and evaporation over periods of days to weeks and introduces a significant element of memory into the land–atmosphere system. Consequently, the availability of reliable information about surface saturation is widely regarded as an important component of accurately forecasting the onset and evolution of flooding events. A portion of this predictability is based on land–atmosphere coupling and on the potential for improving precipitation forecasts through the improved initialization of surface wetness in numerical weather forecasting and climate models [3]. However, a more direct contribution is derived from the increased confidence in runoff and streamflow forecasts afforded by better knowledge of surface infiltration capacity. Regional-scale flooding events are typically associated with extended periods (i.e., weeks to months) of above average rainfall, which steadily erodes the ability of the subsequent rainfall to infiltrate the land surface.

Operational flood forecasting in the United States is currently based on the integration of rainfall and river stage measurements with soil moisture information derived from observed precipitation and simple vertically integrated soil water accounting models [1]. These soil moisture estimates are frequently referenced in flash-flood guidance products generated by United States National Weather Service River Forecast Centers. Satellite remote sensing in general and microwave radiometry in particular can potentially provide reliable and repeated surface (1- to 5-cm depth) soil moisture measurements over lightly and moderately vegetated regions of the globe [4]–[6].

Recent work has demonstrated the increased skill in runoff/rainfall partition modeling when using remotely sensed surface soil moisture [7]–[9]. However, most flooding work has focused on the use of remote sensing as a tool for flood monitoring and assessment instead of for forecasting [10]–[13]. Making the transition between monitoring and forecasting requires direct observations of the hydrologic precursors to flooding events (e.g., elevated soil moisture conditions) and not simply the manifestation of the flood itself.

This letter will attempt to utilize this capability in flood forecasting by examining the value of AMSR-E brightness temperature observations in forecasting the onset and evolution of a flooding event that occurred in northeastern Australia during January 2004. Here, we focus directly on a time series of 6.9 GHz (C-band) and 10.7 GHz (X-band) AMSR-E brightness temperature observations and do not attempt to correct for vegetation water content, surface roughness, or physical temperature impacts on microwave emission. Instead, a time-series methodology is employed that assumes the day-to-day changes in brightness temperature are due primarily to variations in soil water content.

II. Data Synopsis

The AMSR-E instrument aboard the NASA Aqua satellite measures brightness temperature at 6.9, 10.7, 18, 21, 37, and 89 GHz. The spatial resolution on the ground of these observations is 60 km at C- and X-band. This may limit their value for certain applications, but it is important to note that regional-scale flooding events are typically associated with saturated

Manuscript received January 25, 2007; revised August 20, 2007, November 14, 2007, May 12, 2008, and July 14, 2008. Current version published January 14, 2009. This work was supported in part by the NASA EOS Aqua Science program and in part by the NASA Terrestrial Hydrology Program (NASA EOS/03-0204-0265).

R. Bindlish is with Science Systems and Applications, Inc., Hydrology and Remote Sensing Laboratory, Agricultural Research Service, U.S. Department of Agriculture, Beltsville, MD 20705 USA (e-mail: rajat.bindlish@ars.usda.gov).

W. T. Crow and T. J. Jackson are with Hydrology and Remote Sensing Laboratory, Agricultural Research Service, U.S. Department of Agriculture, Beltsville, MD 20705 USA (e-mail: wcrow@hydrolab.arsusda.gov; tjackson@hydrolab.arsusda.gov).

Color versions of one or more of the figures in this paper are available online at http://ieeexplore.ieee.org.

Digital Object Identifier 10.1109/LGRS.2008.2002754

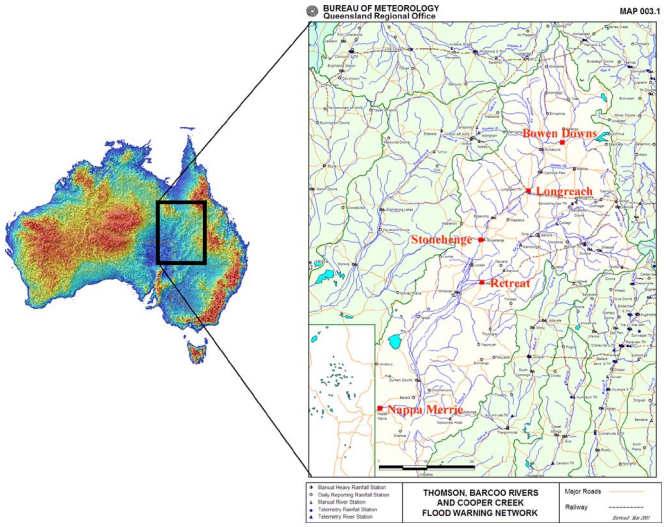

Fig. 1. Map of the Cooper Creek catchment located in Queensland, Australia. Stream gauge locations within the catchment are shown in red.

near-surface conditions over very large areas. More information on the AMSR-E instrument can be found in [4].

The Cooper Creek catchment is located in an arid climate regime and receives an average annual rainfall of less than 400 mm. About half of the annual precipitation occurs during summer due to the monsoons. The Cooper Creek drainage network originates in the Great Dividing Range in northern Queensland and flows into Lake Eyre, South Australia. It has a drainage area of approximately 300 000 km^2. The Cooper Creek is one of three major catchments that comprise the Lake Eyre basin.

Rivers in the catchment are ephemeral, flowing only after significant rainfall and often experiencing long periods of no flow. The southern portion of the catchment is commonly referred to as the "Channel Country" due to the extensive networks of braided and anastomosing channels [14]. Approximately one-third of the Cooper Creek catchment consists of floodplain soils, and the floodplain spans greater than 60 km in the south. Overall, the catchment is a distributary system where annual discharge decreases with increased downstream distance [14]. The large transmission losses responsible for such decreases occur due to a combination of low and patchy rainfall, high evaporation, low topographic gradient, and the presence of numerous potholes in the Channel Country portion of the catchment.

The northern portion of the Cooper Creek catchment consists of the Thompson and Barcoo River watersheds. The Barcoo River drains an area of 50 500 km^2 above the town of Retreat, and the Thompson River drains an area of 87 811 km^2 above the town of Stonehenge (Fig. 1). Unlike the southern portion of the Cooper Creek watershed, both are fast flowing rivers with well-defined channel boundaries and minimal travel times for flood wave propagation. In the Thompson River watershed, there are two operational streamflow gauges at Bowen Downs (22 825 km^2) and Longreach (57 597 km^2), which aid in understanding and monitoring the flood wave propagation (Fig. 1).

The Australian rain gauge network consists of nearly 6000 real-time reporting stations that measure 24-h rainfall accumulations. These observations were interpolated onto a 0.25° latitude–longitude grid using an inverse distance weighting scheme and used to construct a national daily precipitation product for Australia [15].

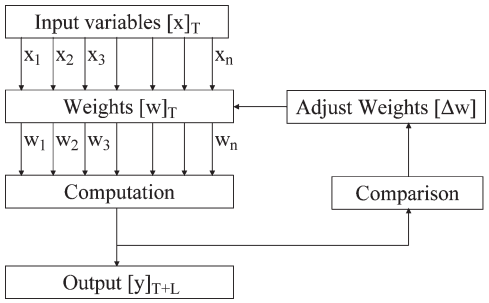

Fig. 2. Schematic of the adaptive model used for streamflow prediction. Observed data from the current and four previous days are used to forecast streamflow with a lead time of five days.

III. Adaptive Streamflow Model

Operational flood forecasts rely on a number of inputs including precipitation observations (or predictions), assessments of land surface infiltration capacity, and the retrospective tuning of model forecasts to match observed streamflow. In order to assess the impact of new observation types on such forecasts, we employ a nonparametric adaptive modeling approach, which—despite its relative simplicity—effectively captures these key aspects of the hydrologic forecasting problem.

A simple statistical adaptive model is developed to forecast streamflow using antecedent precipitation observations, AMSR-E brightness temperature observations and past streamflow rates. These observations form a set of inputs that are weighted using an adaptive model to forecast future streamflow. As they become available, new streamflow observations are used to update these weightings. This adaptive approach is dynamic in nature and can account for nonlinear responses. Essentially, the adaptive model performs a linear fit at a given instant of time. However, these weights change depending on evolving prevalent conditions. These changes allow the model to adaptively update itself in response to dynamic changes in forecasting performance and outperform simpler regression approaches based on a single static fit of observations to observed streamflow. In this way, streamflow is forecast for time $t + L$ using observations available at time t and streamflow forecasts for times $t + 1$ to $t + L - 1$, where L represents the lead time for the forecasts. The forecast lead time (response time) depends on the geophysical characteristics of the watershed and is independent of the precipitation event. Here, the lead time is determined using the typical lag between observed precipitation and streamflow response.

Fig. 2 shows a schematic of the adaptive model. The input $[X(t)]$ consists of precipitation $[P(t)]$, brightness temperature $[\mathrm{Tb}(t)]$, and streamflow $[S(t)]$ observations. Brightness temperature, precipitation, and observed streamflow for five time steps (i.e., the present and four previous days) are used in the adaptive model. Based on time series analysis, a forecast is made for the next five days ($L = 5$ days) using the adaptive model. Therefore, the input vector $X(t)$ is expressed in (1), shown at the bottom of the next page, where $Y(t)$ represents streamflow forecasts obtained through previous applications of the adaptive model. AMSR-E brightness temperatures at 6.9 and 10.7 GHz for both H and V polarizations were used in

the adaptive model. Streamflow forecasts for time $t+L$ are obtained using

$$Y(t+L) = X(t) \bullet W(t). \tag{2}$$

As they become available, streamflow observations $S(t)$ are compared to streamflow forecasts $Y(t)$ (obtained L days in the past), and their difference is used to update $W(t)$ [16]

$$W(t+1) = \frac{[Y(t) - S(t)]}{\sum W(t)X(t)} * X(t) \bullet W(t) + W(t). \tag{3}$$

Data from January to March 2003 were used to initialize the model weights. Following this initialization, streamflow forecasts were made using (2) and weightings iteratively updated using comparisons with streamflow observations as given by (3). In this way, (2) and (3) comprise a simple adaptive approach to streamflow forecasting. Since the Cooper Creek watersheds have little or no baseflow component, the adaptive model was turned off (until the next precipitation event) once forecasts of zero or negative streamflow were made. This area receives significant precipitation resulting in streamflow only during the summer.

It is important to note that (2) describes a nonparametric approach to forecasting streamflow observations. Since it lacks a basis in hydrologic modeling, it cannot be applied to other watersheds without adequate calibration. In particular, the weighting vector calculated in (3) is site-dependent and must be obtained on an individual basis for each watershed.

IV. Event Evolution

Heavy and persistent monsoonal rains during January 2004 produced the wettest January in 30 years for the Australian state of Queensland. Percentage comparison to normal shows the extremity of the flooding event, with large areas of the Barcoo River watershed receiving 300%–400% of normal rainfall for the period. This precipitation spawned the worst flooding since 1972 and resulted in 32 million U.S. dollars of damage. Widespread precipitation began on January 9 in the northern part of the Barcoo watershed (areal average of 30 mm/day). This precipitation event was followed by another event from January 12–14 (areal average of 90 mm/day). Fig. 3 shows the 6.9 H GHz AMSR-E observations over northeastern Australia during this period. As a result of these precipitation events, brightness temperature observations over the region decreased (indicating a rise in soil moisture) until they reached a minimum between January 13 and 17.

In contrast, streamflow in the Barcoo River and Cooper Creek was below flood levels prior to January 13. Moderate to minor flooding was observed on January 14 along the Barcoo River [Fig. 4(b)]. Major flooding was not detected until January 15, and peak flows did not occur until January 18. In the town of Retreat, Queensland, the Barcoo River crested on January 18 at 11 m, 8 m above the 3-m flood stage. Since peak flows in the Barcoo River did not occur until January 18, it is clear that the minimum brightness temperatures (i.e., highest soil moistures) in Fig. 3 precede peak streamflow conditions by about four days. Similar lead times were observed along the Thompson River. The upstream gauge at Bowen Downs had a somewhat shorter lead time (four days) than downstream gauges at Longreach and Stonehenge (six days). Nevertheless, the brightness temperature signatures of inundated land surface conditions shown in Fig. 3 constitute a remotely detectable precursor to subsequent downstream flooding.

The use of microwave sensors provides a unique opportunity to monitor the land surface in the presence of clouds. This ability is critical for flood forecasting since rainy periods preceding the onset of large-scale flooding naturally tend to be associated with extensive cloud cover. This limits the value of visible/infrared sensors for flood forecasting and monitoring purposes. Remote visible and infrared sensors provide higher resolution imaging during cloud-free days, but it is critical to supplement these images with microwave observations on cloudy days. For this particular event, the Moderate Resolution Imaging Spectroradiometer could not image this flooding event until after the onset of widespread major flooding on January 18.

After peak flooding during the middle of the month, the Cooper Creek catchment did not receive significant precipitation during the second half of January 2004. A dry-down pattern (increasing brightness temperatures) can be seen during this period in the AMSR-E brightness temperature imagery in Fig. 3. The areal average 6.9 H GHz brightness temperature increased from $\sim$218 to $\sim$260 K during the period. This increase is partly due to an increase in surface temperature. Nevertheless, catchment-averaged brightness temperatures at the end of January were still lower than preevent levels and did not rise back to such levels (i.e., $\sim$270 K before January 7) until February 1. After January 24, 2004, an area of low brightness temperature (associated with the flood wave) propagated very slowly downstream over a period of about 20 days, finally reaching Nappa Merrie around February 15 (Fig. 3). The extremely slow propagation speed below Retreat is due to the presence of extensively braided channels and numerous sinkholes along the lower reaches of the Copper Creek catchment [14].

V. Modeling Results

Fig. 4(a) shows the time series of areal average precipitation and brightness temperature observations over the Barcoo River watershed. Significant precipitation over the watershed started on January 6, which resulted in wet surface soil moisture conditions (i.e., low brightness temperatures). This was followed by another event starting on January 9, which resulted in nearly saturated soil moisture conditions. This wetting is clearly visible in C-band AMSR-E imagery (Fig. 3) and time series data in Fig. 3 which indicate a decrease of $\sim$52 K in watershed-averaged brightness temperature between January 6 and 13.

$$X(t) = \begin{bmatrix} \underset{i=t-L+1}{\overset{i=t}{P(i)}} & \underset{i=t-L+1}{\overset{i=t}{\mathrm{Tb}_{6H}(i)}} & \underset{i=t-L+1}{\overset{i=t}{\mathrm{Tb}_{6V}(i)}} & \underset{i=t-L+1}{\overset{i=t}{\mathrm{Tb}_{10H}(i)}} & \underset{i=t-L+1}{\overset{i=t}{\mathrm{Tb}_{10V}(i)}} & \underset{i=t-L+1}{\overset{i=t}{S(i)}} & \underset{i=t+1}{\overset{i=t+L-1}{Y(i)}} \end{bmatrix} \tag{1}$$

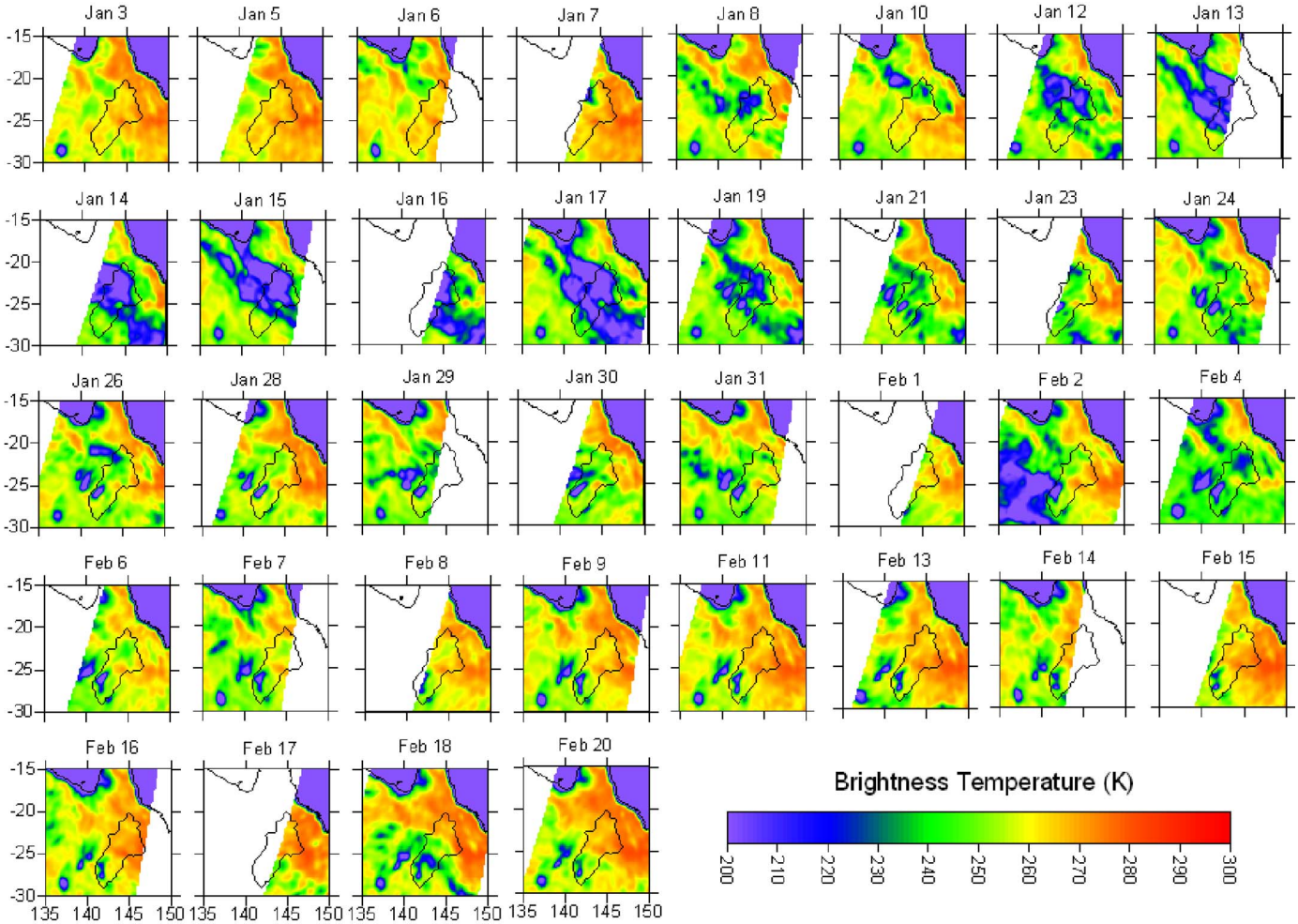

Fig. 3. AMSR-E H 6.9 GHz observations over northeastern Australia during January–February 2004. All the images are for the 1:30 A.M. (local time) overpass time. The figures show the Cooper Creek catchment boundary at Nappa Merrie (drainage area—236 985 km^2).

Brightness temperature reached a minimum on January 13, four–five days prior to the peak flooding at Retreat. An additional 50 mm of precipitation fell on January 13–14. This precipitation event, occurring on soils already saturated by preceding storms, led to very efficient runoff generation and the onset of flooding in the watershed. However, streamflow in the watershed did not reach the major flood stage until January 18. The approximately five-day time lag between peak precipitation and discharge was used to define L for the adaptive streamflow model (Section III and Fig. 2).

The adaptive model was run with $L = 5$ days to forecast streamflow for the Barcoo watershed using both precipitation and brightness temperature inputs [Fig. 4(b)]. The model matched the observations very well in terms of the peak magnitude of the flood wave. The predicted peak streamflow was 87% of the observations.

To study the incremental value of AMSR-E brightness temperature observations over precipitation observations alone, a data denial study was performed in which the adaptive model was run with no brightness temperature observations [Fig. 4(b)]. The model was reinitialized by using only the precipitation observations. Neglecting all brightness temperature observations leads to a slightly better prediction of peak streamflow intensity by the adaptive model but causes a large underestimation of total flood wave volume. The use of brightness temperature in the adaptive model provides an assessment of antecedent infiltration capacity (based on soil moisture memory of past rainfall), which, in turn, enables the adaptive model to accurately predict the total volume of the flood wave. However, no comparable advantage is noted for flood peak (as opposed to flood volume) forecasting.

A two-week period without significant precipitation followed peak flooding on January 18. This resulted in a dry-down throughout the Barcoo River watershed during which brightness temperatures increased to preflooding levels by February 1. However, the watershed received about 30 mm of additional precipitation on February 4. In the data denial (precipitation only) analysis, this resulted in a large overprediction of streamflow ($\sim$300% of observed streamflow) on February 12 not observed in the modeling results using precipitation and brightness temperature [Fig. 4(b)]. The lack of streamflow response to precipitation was due to the absence of saturated conditions preceding the precipitation event. During this period, land surface information contained in the AMSR-E brightness temperature fields allows the adaptive model to avoid a false positive flooding prediction by correctly capturing dry antecedent conditions not conducive to heavy runoff generation.

Similar results were obtained when the model was used over other subwatersheds in the Cooper Creek catchment. The model was run using streamflow observations for Bowen Downs,

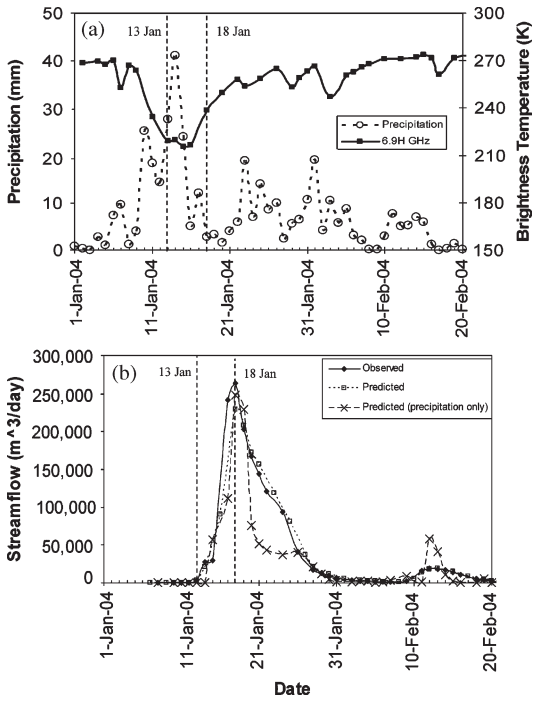

Fig. 4. (a) Observed precipitation and areal averaged brightness temperature observations for the Barcoo watershed at Retreat (drainage area of 50 500 km^2). (b) Observed and predicted streamflow observations for the Barcoo river watershed. Streamflow forecasts are made using both brightness temperature and precipitation observations and a precipitation-only case in which brightness temperature is neglected. Dates for the onset of saturated land surface conditions (January 13, 2004) and observed peak streamflow (January 18, 2004) are indicated.

Longreach, Stonehenge, Retreat, and Nappa Merrie. Only results from the Barcoo River at Retreat are presented here.

VI. Discussion and Conclusion

Two characteristics of microwave remote-sensing observations make them uniquely valuable for flood forecasting. First, microwave observations are sensitive to soil moisture conditions and, thus, can detect antecedent surface conditions conducive to efficient runoff generation and the development (or intensification) of regional-scale flooding events. Second, microwave observations are capable of penetrating cloud cover, which is typically extensive before, during, and after regional flooding events.

The physical basis of this forecasting approach is that remotely sensed surface soil moisture contains information on current surface saturation conditions and, consequently, helps to predict the future response of the land surface to precipitation. This type of information will be of value for large-scale flooding events (> 5000 km^2) in which the gradual build-up of antecedent soil moisture (over days to weeks) due to consistently heavy precipitation is a detectable precursor to the onset of actual flooding. It is likely that the observed brightness temperature does not correlate well with streamflow observations for complex watersheds. It will also be of relatively less value for flash flood events driven by extreme levels of precipitation occurring over relatively fine space-time scales or floods resulting from sudden snow melt.

Microwave observations of the January 2004 Queensland flooding event show the clear development of saturated land surface conditions in the days prior to the precipitation event that triggered the flooding event (Fig. 3). Through the use of an appropriate adaptive streamflow model, these observations can be used to improve the quality of streamflow forecasts made during and after the flooding event (Fig. 4). In this way, AMSR-E observations provide additional, as opposed to simply redundant, skill relative to forecasts obtained with only rainfall observations. The potential value of remotely sensed observations is particularly high for catchments lacking good streamflow and ground-based rainfall instrumentation. Future research will address these issues by systematically applying the approach to a wider range of flooding events in large-scale basins with a variety of climatic and land cover characteristics. Future lower frequency L-band missions (SMOS and SMAP) are expected to further enhance the value of remotely sensed soil moisture products for hydrologic forecasting applications.

References

[1] NRC, *Assessment of Hydrologic and Hydrometeorological Operations and Services*, 1996, Washington, DC: Nat. Academy Press.

[2] IPCC, *Climate Change 2001, Contributions of the Working Group II to the Third Assessment Report of the International Panel on Climate Change*, 2001, Cambridge, U.K.: Cambridge Univ. Press.

[3] R. D. Koster *et al.*, "Regions of strong coupling between the soil moisture and precipitation," *Science*, vol. 305, no. 5687, pp. 1138–1140, Aug. 2004.

[4] E. G. Njoku, T. J. Jackson, V. Lakshmi, T. K. Chan, and S. V. Nghiem, "Soil moisture retrieval from AMSR-E," *IEEE Trans. Geosci. Remote Sens.*, vol. 41, no. 2, pp. 215–229, Feb. 2003.

[5] T. J. Jackson, "Soil moisture estimation using special satellite microwave/imager satellite data over a grassland region," *Water Resour. Res.*, vol. 33, no. 6, pp. 1475–1484, 1997.

[6] R. Bindlish, T. J. Jackson, E. F. Wood, H. Gao, P. Starks, D. Bosch, and V. Lakshmi, "Soil moisture estimates from TRMM Microwave Imager observations over the Southern United States," *Remote Sens. Environ.*, vol. 85, no. 4, pp. 507–515, Jun. 2003.

[7] R. N. Pauwels, R. Hoeben, N. E. C. Verhoest, F. R. De Troch, and P. A. Troch, "Improvement of TOPLATS-based discharge predictions through assimilation of ERS-based remotely sensed soil moisture values," *Hydrol. Process.*, vol. 16, no. 5, pp. 995–1014, Apr. 2002.

[8] J. M. Jacobs, D. A. Myers, and B. M. Whitfield, "Improved rainfall/runoff estimates using remotely sensed soil moisture," *J. Amer. Water Resour. Assoc.*, vol. 39, no. 2, pp. 313–324, Apr. 2003.

[9] W. T. Crow, R. Bindlish, and T. J. Jackson, "The added value of spaceborne passive microwave soil moisture retrievals for forecasting rainfall–runoff partitioning," *Geophys. Res. Lett.*, vol. 32, no. 18, L18 401, Sep. 2005. DOI:10:1019/2005GL023543.

[10] D. E. Alsdorf, J. M. Melack, T. Dunne, L. A. K. Mertes, L. L. Hess, and L. C. Smith, "Interferometric radar measurements of water level changes on the Amazon flood plain," *Nature*, vol. 404, no. 6774, pp. 174–177, Mar. 2000.

[11] P. A. Brivio, R. Colombo, M. Maggi, and R. Tomasoni, "Integration of remote sensing data and GIS for accurate mapping of flooded areas," *Int. J. Remote Sens.*, vol. 23, no. 3, pp. 429–441, Feb. 2002.

[12] A. Freeman, B. Chapman, and P. Siqueira, "The JERS-1 Amazon Multi-season Mapping Study (JAMMS): Science objectives and implications for future missions," *Int. J. Remote Sens.*, vol. 23, no. 7, pp. 1447–1460, 2002.

[13] R. Scofield, J. G. LaDue, R. Scofield, N. Grody, and R. Ferraro, "A soil wetness index for monitoring the great flood of 1993," in *Proc. 7th Conf. Satellite Meteorol. Oceanography*, 1994, pp. 580–583.

[14] A. D. Knighton and G. C. Nanson, "Flow transmission along an arid zone anastomosing river, Cooper Creek, Australia," *Hydrol. Process.*, vol. 8, no. 2, pp. 137–154, Mar. 1994.

[15] G. Weymouth, G. A. Mills, D. Jones, E. E. Ebert, and M. J. Manton, "A continental scale daily rainfall analysis system," *Aust. Meteorol. Mag.*, vol. 48, pp. 169–179, 1999.

[16] S. Haykin, *Adaptive Filter Theory*. Englewood Cliffs, NJ: Prentice–Hall, 2001.